Int. J. Electrochem. Sci., 7 **(2012)** 3798 - 3808

International Journal of
ELECTROCHEMICAL
SCIENCE
www.electrochemsci.org

Synthesis and Physicochemical Properties of Nanomagnetic Zinc Ferrite System

N. M. Deraz[1,2,*] *and A. Alarifi*[1]

[1] Catalytic chemistry chair, Chemistry Department, College of Science, King Saud University, Riyadh, Saudi Arabia
[2] Physical Chemistry Department, Laboratory of Surface Chemistry and Catalysis, National Research Center, Dokki, Cairo, Egypt
[*]E-mail: nmderaz@yahoo.com

Received: 27 March 2012 / *Accepted:* 11 April 2012 / *Published:* 1 May 2012

Effects of various amounts of fuel on structural, morphological and magnetic properties of $ZnFe_2O_4$ nano-particles have been studied. The specimens were characterized by IR, XRD, SEM, TEM and VSM. The XRD measurements confirm the formation of well-crystalline zinc ferrite as a single phase. Transmission electron microscopy analysis revealed the formation of Zn-ferrite particles with a narrow size distribution in the range of 40- 58 nm. The change in the fuel to oxidant ratio results in an increase of both the magnetization and coercivity of the as prepared nano-particles. This observation implies that, besides size, m causes also significant structural rearrangements which in turn induce changes in the strength and the number of Fe^{3+}(A)–O–Fe^{3+}(B) superexchange interactions.

Keywords: IR; SEM; TEM; M_s and H_c

1. INTRODUCTION

The physicochemical properties of materials can be tuned by controlling the particle size, shape and the inter-particle interactions [1–4]. Due to potential applications of nano-materials, several new synthesis routes for the production of nano-crystals with desired properties have been developed [5–11]. Recently, a significant growth in the study of ferrite based nano-materials due to their surface and quantum confinement effects which affect their physical and chemical properties. Magnetite and spinel ferrite nano-crystals are regarded as one of the most important inorganic nano-materials because of their electronic, optical, electrical, magnetic and catalytic properties which are different from their bulk counterparts. So, the ferrite materials have been extensively used in various technological applications.

It is a well-known fact that the properties of ferrite materials are strongly influenced by the materials' composition, microstructure, preparation methodology, impurity levels and sintering conditions which are sensitive to the preparation methodology [12, 13]. These ferrites are usually prepared by the conventional ceramic method, in which the stoichiometric composition and final microstructure are extremely difficult to control. This method requires prolonged heating at high temperatures during preparation leading to evaporation of some the constituents, with subsequent modification in the desired stoichiometry. In addition, the volatilization of zinc at high temperatures results in the formation of Fe^{2+} ions, which increase electron hopping and reduce resistivity during the preparation of zinc ferrite [14].

Indeed, the selection of an appropriate process for the preparation method is the key to obtain good quality ferrites. So, various preparation techniques have been developed to produce $ZnFe_2O_4$ nanoparticles, e.g. precipitation, microemulsion, hydrothermal, thermal decomposition, ball milling, polyol, and co-precipitation methods [15-18]. Each of these techniques has its own merits and demerits. Among various synthesis routes, combustion technique is one of the most convenient and versatile methods for the preparation of $ZnFe_2O_4$ nanoparticles [19].

Neutron diffraction studies were reported that bulk $ZnFe_2O_4$ which crystallizes in the normal spinel structure containing two different cation sites, 8 tetrahedral A sites occupied by Zn^{2+} ions and 16 octahedral B sites occupied by Fe^{3+} ions [20]. The structural and magnetic properties of ferrite based materials are influenced by preparation method and thermal treatment [21]. Schäfer et al. [22] have reported from powder neutron diffraction studies that the magnetic properties of ZnFe2O4 compounds are: (i) antiferromagnetic long range order below 10.5 K if the sample was annealed and slowly cooled; (ii) absence of any long range order for the sample annealed and quenched; (iii) onset of ferromagnetic ordering at 500 K for nanocrystalline material.

In this context, the combustion route is advantageous over the solid state synthesis in terms of better compositional, homogeneity and purity of the final product. In addition, a few efforts have been made to correlate the effect of synthesis parameters like fuel-to-oxidant ratio with powder characteristics especially in the case of zinc ferrite [23, 24]. So, this effort has been made to identify the effect of fuel ratios on structural, morphology, magnetic properties and production of zinc ferrite.

2. EXPERIMENTAL

2.1. Materials

Zinc ferrite samples were prepared by mixing calculated proportions of zinc and ferric nitrates with different amounts glycine. The mixed precursors were concentrated in a porcelain crucible on a hot plate at 350 ^{o}C for 5 minutes. The crystal water was gradually vaporized during heating and when a crucible temperature was reached, a great deal of foams produced and spark appeared at one corner which spread through the mass, yielding a voluminous and fluffy product in the container. In our experiments, The as-prepared solid samples have been designated as Z1, Z2 and Z3 containing the ratio of the Glycine: Zn $(NO_3)_2.6H_2O$: $Fe(NO_3)_3.9H_2O$ were (2, 6 and 12) : 1 : 2, respectively. On the

other hand, the ratios of fuel (glycine, G) to cations (or nitrate, N) were 0.67, 2 and 4 for Z1, Z2 and Z3, respectively. All samples were calcined in air at 700 ^{o}C for 1h. The chemicals employed in the present work were of analytical grade supplied by Prolabo Company.

2.2. Techniques

An X-ray measurement of various mixed solids was carried out using a BRUKER D8 advance diffractometer. The patterns were run with Cu K_α radiation at 40 kV and 40 mA with scanning speed in 2θ of 2 ° min^{-1}.

The crystallite size of Zn-ferrite present in the investigated solids was based on X-ray diffraction line broadening and calculated by using Scherrer equation [25].

$$d = \frac{B\lambda}{\beta \cos\theta} \qquad (1)$$

where d is the average crystallite size of the phase under investigation, B is the Scherrer constant (0.89), λ is the wave length of X-ray beam used, β is the full-with half maximum (FWHM) of diffraction and θ is the Bragg's angle.

An infrared transmission spectrum of various solids was determined using Perkin-Elmer Spectrophotometer (type 1430). The IR spectra were determined from 1000 to 350 cm^{-1}. Two mg of each solid sample were mixed with 200 mg of vacuum-dried IR-grade KBr. The mixture was dispersed by grinding for 3 min in a vibratory ball mill and placed in a steel die 13 mm in diameter and subjected to a pressure of 12 tonnes. The sample disks were placed in the holder of the double grating IR spectrometer.

Scanning electron micrographs (SEM) and Transmission electron micrographs (TEM) were recorded on JEOL JAX-840A and JEOL JEM-1230 electron microanalyzers, respectively. The samples were dispersed in ethanol and then treated ultrasonically in order disperse individual particles over a gold grids.

The magnetic properties of the investigated solids were measured at room temperature using a vibrating sample magnetometer (VSM; 9600-1 LDJ, USA) in a maximum applied field of 15 kOe. From the obtained hysteresis loops, the saturation magnetization (M_s), remanence magnetization (M_r), coercivity (H_c) and magnetic moment (n_B) were determined.

3. RESULTS AND DISCUSSION

3.1. IR studies

Fig. 1 shows the IR spectrums of different zinc ferrite samples in the range of 350 -1000 cm^{-1}. The zinc ferrites crystallize in spinel form with the space group *Fd*3*m* [20]. The spinel ferrites are

known to exhibit four fundamentals IR active modes in the vibration spectra. In the present study, the absorption bands for the synthesized ferrites are in the expected range. The pure $ZnFe_2O_4$ shows absorption bands at 545±4 and 410±3 cm^{-1}. According to Waldron [26], the high frequency band v_1 around 545 cm^{-1}, the low frequency band v_2 around 410 cm^{-1} is attributed to that of tetrahedral and octahedral complexes, respectively. The variation in the band positions is due to the difference in the Fe^{3+}–O^{2-} distances for the octahedral and tetrahedral complexes.

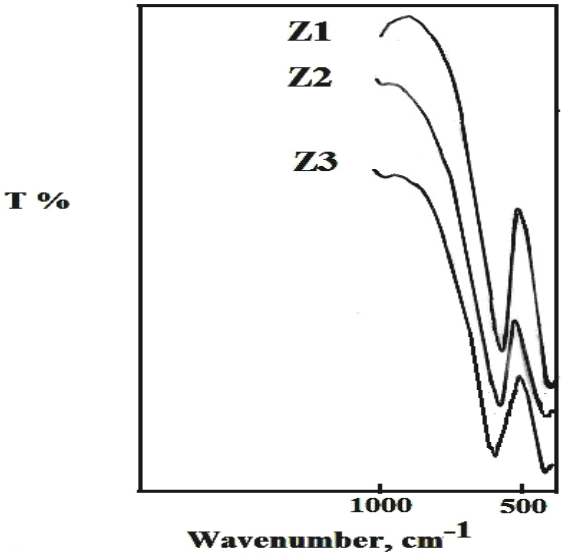

Figure 1. X-ray diffraction patterns of Z1, Z2 and Z3 samples.

The change in the G/N ratio brought about the shifts in the positions of the frequency bands towards lower wave number due to the increase in particle size [27]. As the particle size increases, the increase in frequency is observed [28]. The difference in the positions of the absorption bands, v_1 and v_2, is referred to change in the formation of zinc ferrite by the G/N ratio depending upon the method and conditions of preparation.

3.2. XRD analysis

The XRD patterns of different $ZnFe_2O_4$ powders synthesized by the combustion technique are depicted in Fig. 2. All the characteristic peaks of $ZnFe_2O_4$ (Franklinite) are present in the investigated diffraction pattern. In all samples, the single phase spinel structure of $ZnFe_2O_4$ is formed by combustion technique followed by heat treatment at 700 ^oC for 1h. However, a sharp increase in the crystalline nature (the height of peaks) of the zinc ferrite powders is observed as the amount of glycine was increased, which is recorded as a decrease in the broadening of the peaks in the diffraction patterns. This clearly indicates that the zinc ferrite formation has increased with increase of glycine added. In other words, the treatment of mixture of zinc and iron nitrates with glycine as fuel supplies

larger motion force for the formation of the ferrite phase with larger crystallinity via complete conversion of any un-reacted oxides [14].

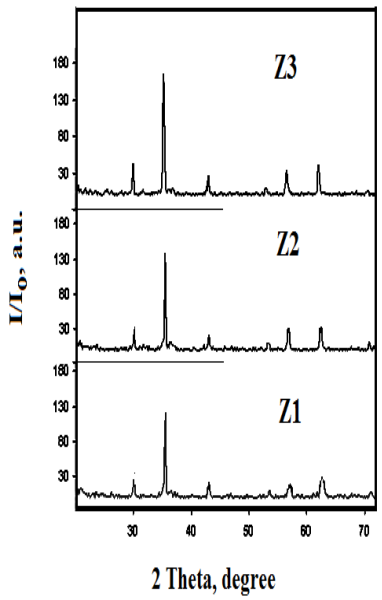

Figure 2. XRD patterns of Z1, Z2 and Z3 samples.

An X-ray data enable us to investigation the role of G/N ratio in modifying the structural parameters such as the crystallite size (d), lattice constant (a), unit cell volume (V) and X-ray density (D_x) for the produced zinc ferrite solids. The values obtained of various structural parameters are given in Table 1.

Table 1. Effects of the G/N ratio on some structural parameters of zinc ferrite phase.

Samples	G/N ratio	d (nm)	a (nm)	V (nm^3)	D_x (g/cm^3)
Z1	0.67	40	0.8380	0.5885	5.4455
Z2	2.00	47	0.8399	0.5925	5.4088
Z3	4.00	58	0.8419	0.5967	5.3707

It can be seen from this table that the increase in the G/N ratio brought about an increase in the values of a, d and V. However, this treatment led to a decrease in the density of zinc ferrite compound. The decrease in the density of zinc ferrite may be due to the increase in glycine content could be attributed to the reduction of oxygen vacancies which play a predominant role in accelerating densification i.e. the decrease in oxygen ion diffusion would retard the densification. It is reported that the diffusion of oxygen ions, which have a larger diameter than the cations, is the major factor which determines the rate of sintering of ferrites. The observed increase in the crystallite size, lattice constant

and unit cell volume could be attributed to the agglomeration and/or grain growth of nano-sized zinc ferrite particles produced. This will confirm by SEM and TEM techniques.

Peaks dislocation was observed according to the increase in the G/N ratio. This occurs due to the ionic radius input difference of the reacted oxides. However, the treatment of our samples with different amounts of glycine led to an increase in the crystallite size from 40 to 58 nm depending upon the increase in lattice constant from 0.8380 to 0.8419 nm. This could be attributed to the grain growth of the prepared particles and/or the substitution of some Fe^{3+} species (0.064nm) by Zn^{2+} species (0.074nm) via the migration of Fe^{3+} species from B to A sites. This migration could be lead to expansion in the zinc ferrite lattice with subsequent increase in its crystallite size. This speculates can be confirmed from the change observed in the intensities of the (2 2 0), (4 4 0) and (5 1 1) planes which are more sensitive to the cations on tetrahedral, octahedral and the oxygen ion parameters, respectively [14].

Table 2. Effects of the G/N ratio on the intensity values of hkl planes of $ZnFe_2O_4$ phase.

Samples	G/N ratio	Peak height (a. u.)		
		I_{220}	I_{551}	I_{440}
Z1	0.67	50	30	33
Z2	2.00	55	35	37
Z3	4.00	60	37	41

Table 2 displays the observed intensities of the above three planes. It can be observed that the intensity of the (2 2 0) and (4 4 0) planes increases with the continuous addition of glycine, which infers that the Zn^{2+} and Fe^{3+} ions have preferentially occupied the A and B sites, respectively. But, the maximum increase in the intensity of the (2 2 0) and (4 4 0) planes attained 20% and 24.2%, respectively. This indicates that the increase in the intensity of the (2 2 0) plane is smaller than that of the (4 4 0) plane. This could be attributed to the increasing amounts of zinc ions at B sites involved in the zinc ferrite lattice. Thus, we can conclude that the content of Zn^{2+} ions at the B site increases via the migration of Fe^{3+} and Zn^{2+} from B and A sites to A and B sites, respectively [14]. In other words, the treatment with glycine at 350 ^{o}C brought about an increase in the number of Zn^{2+} ions on B site with increasing of the crystallite size, lattice constant and unit cell volume. This finding indicates the promotion effect of the increasing amount of glycine in the formation of partially inverted cubic spinel structure of zinc ferrite. On the basis of the above data and on earlier studies [29], the spinel structure can be assigned in the synthesized materials can be expressed as

$$(Zn_{1-\delta}{}^{2+}\ Fe_{\delta}{}^{3+})_A[Zn_{\delta}{}^{2+}\ Fe_{2-\delta}{}^{3+}]_B\ O_4{}^{2-} \qquad (2)$$

where δ is the inversion parameter. In the case of normal spinel δ = 1 and for inverse spinel δ = 0 [30]. For partly inverted spinel δ is in between 0 and 1. The crystalline bulk form of $ZnFe_2O_4$ is a normal spinel with Zn^{2+} ions only on the A sites and Fe^{3+} ions only on the B sites. Recent investigations of nanocrystalline $ZnFe_2O_4$ have suggested that the cation distribution in this material is partly inverted and exhibits anomaly in its magnetization [31]. In addition, the above equation emphasizes the influence of the δ values on the formation of zinc ferrite, morphological, structural and magnetic properties of zinc ferrite.

3.3. SEM and TEM studies

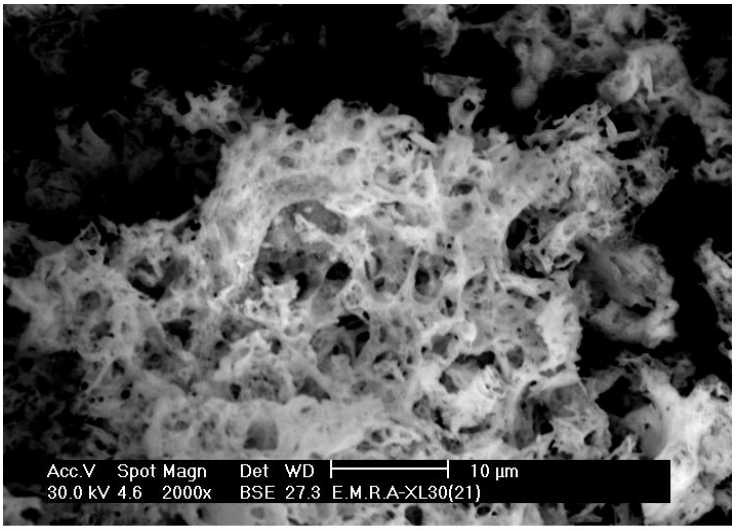

A

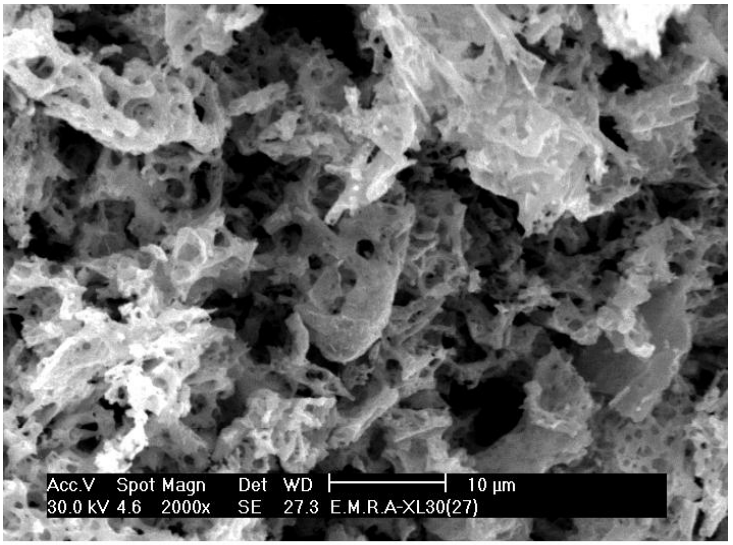

B

Figure 3. SEM images for (a) Z1 and (b) Z3 specimens.

The Scanning electron microscope, SEM, images given in Fig. 3a and b of Z1 and Z3 specimens reveal remarkable changes in the microstructure and porosity. One can see the formation of

spongy and fragile network structure. The voids and pores present in the samples are attributed to the release of large amount gases during combustion process. Also, SEM micrograph of the Z3 sample (Fig. 3b) contains fracture surfaces of the aggregated powders.

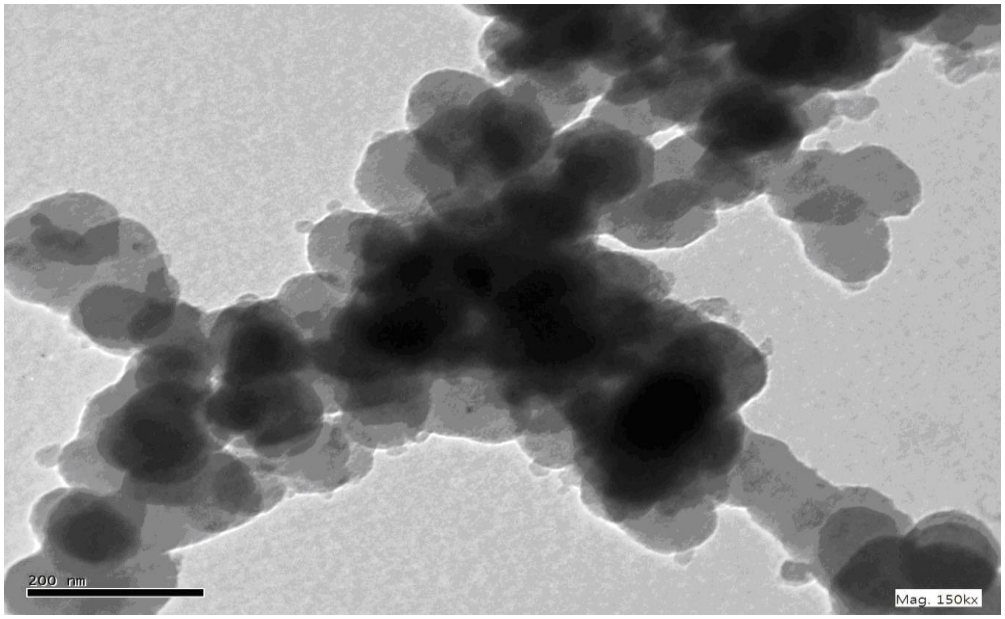

A

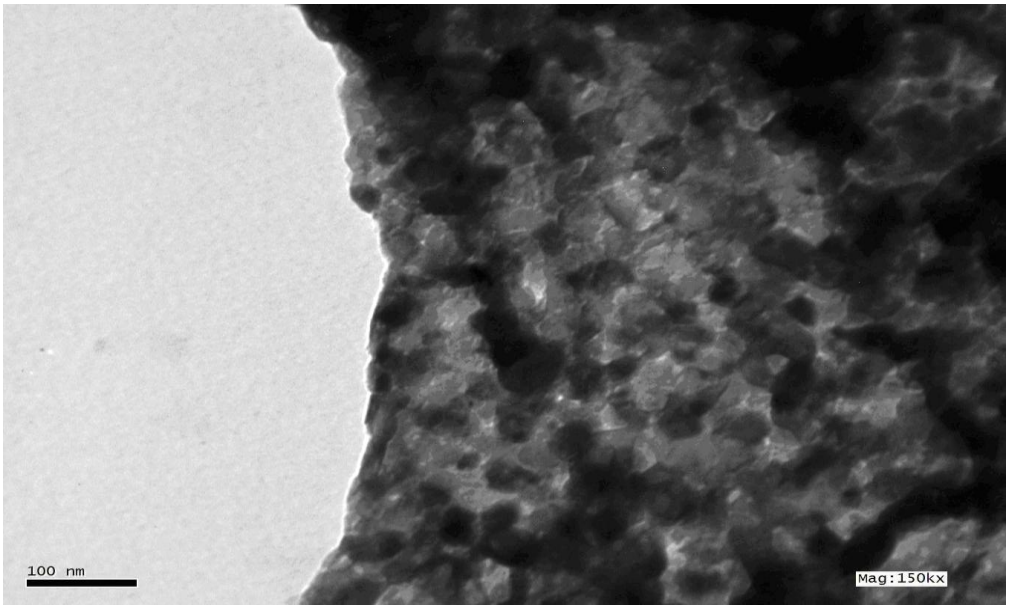

B

Figure 4. TEM images for (a) Z1 and (b) Z3 specimens.

The transmission electron microscope, TEM, images of Z1 and Z3 specimens are given in Fig. 4a and b. TEM image indicates that the Z3 sample has polyhedron particles (Fig. 4b) while the Z1 sample contains spherical particles (Fig. 4a) with uniform grain size distribution. The average particle size of the synthesized solids varies from 40 to 58 nm by increasing the G/N ratio, which is a good

agreement with the average crystallite size determined by XRD analysis. This finding speculated that the as synthesized zinc ferrite consisted entirely of well nano-crystalline particles. In addition, this suggests several neighboring particles fuse together to increase particle sizes by melting their surfaces [32].This grain growth of particle size enlargement at higher G/N ratio has been observed previously in various ferrites and in zinc ferrite systems [33, 34]. Finally, the electron micrograph of the Z3 sample (Fig. 4b) consisted of agglomerated grains with visible grain boundaries.

3.4. Magnetic studies

The magnetization of spinel zinc ferrites originates from the difference in the magnetic moments of the ions at the octahedral lattice sites and those at the tetrahedral lattice sites, and thus directly reflects the distribution of the magnetic Fe^{3+} and non-magnetic Zn^{2+} ions between the two sublattices. In fact, the magnetic properties of zinc ferrite materials are influenced mainly by the preparation route, cation distribution, grain size and sintering conditions [35]. The specific magnetization curves of the investigated samples, obtained from room temperature VSM measurements, are shown in Fig. 5.

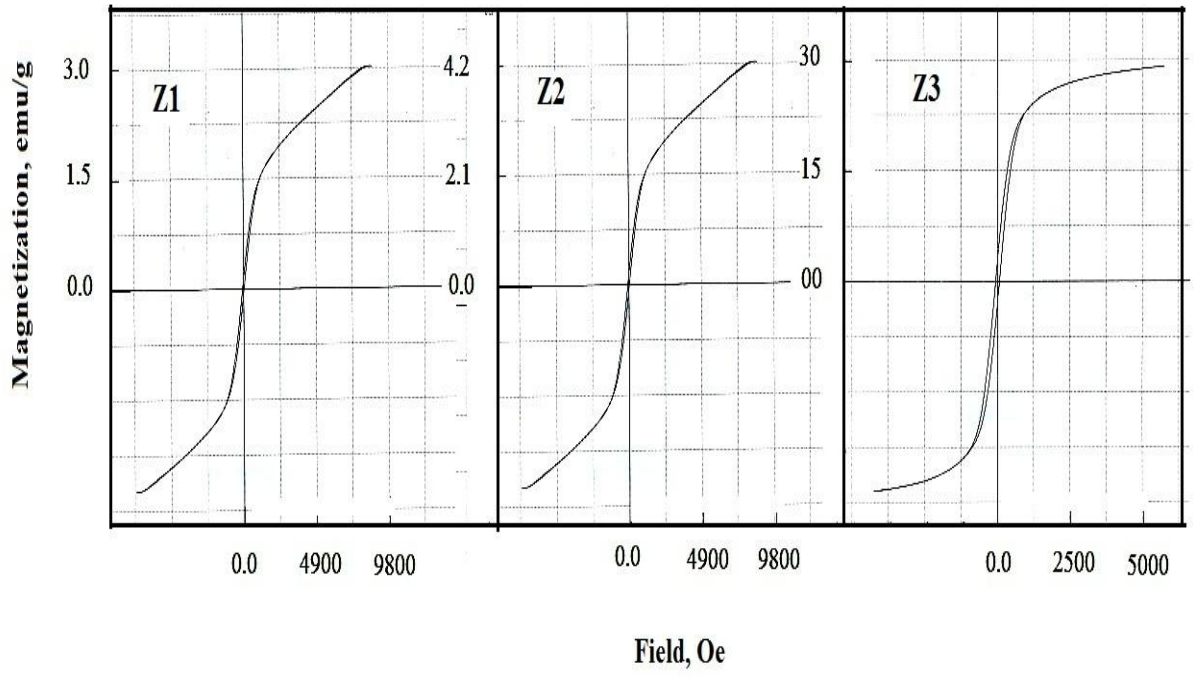

Figure 5. Magnetic hysteresis curves measured at a room temperature for Z1, Z2 and Z3 samples.

From these measurements, the magnetization and the coercivity are derived and listed in Table 3. It can be seen from figure 5 and Table 3 that: (i) the magnetization of zinc ferrite nano-particles changes with the change in the G/N ratio. The increase in the G/N ratio up to 4 resulted in a significant increase in the saturation magnetism (M_s) of zinc ferrite. (ii) An increase of the G/N ratio from 0.67 to

4 led to an increase in the coercivity (Hc). (iii) As the G/N ratio increases, the magnetic moment (n_B) increases. These findings with the increase in the grain size can be explained on the basis of domain structure, critical diameter and the anisotropy of the crystal [36, 37].

Table 3. Effects of the G/N ratio on the magnetic properties of the as-prepared solids.

Samples	G/N ratio	M_s (emu/g)	M_r (emu/g)	M_r/M_s (emu/g)	H_c (Oe)	n_B
Z1	0.67	2.91	0.07	0.024	5.2	0.126
Z2	2.00	4.16	0.545	0.131	52.6	0.180
Z3	4.00	29.06	8.18	0.281	75.1	1.255

The augmentation in magnetization of zinc ferrite with an increase in the amount of glycine added is expected since the ‘‘extra’’ magnetic Fe ion will incorporate at the tetrahedral sublattice leading to an increase in the magnetic moment. This suggests higher strength Fe^{3+}(A)–O–Fe^{3+}(B) interactions [38].

4. CONCLUSIONS

Nano-crystalline zinc ferrite was produced by flash combustion process. In this process, metal nitrates were used as raw materials in presence of glycine as fuel. The structure, morphology and magnetic properties of as prepared samples were investigated by XRD, IR, SEM, TEM and VSM techniques. The obtained results revealed that the fuel to oxidant ratio is possible to control the structural characteristics, porosity and grain size which can influence the magnetic properties of ferrites. The grain sizes of the formed ferrites were 30-40 nm, that is much smaller than these obtained by classical method. Consequently, the flash combustion procedure is promising for producing ultra fine-grained zinc ferrites

ACKNOWLEDGEMENT
This work was supported by NPST program by King Saud University Project: Number 09-ADV651-02.

References

1. C. Burda, X. Chen, R. Narayanan, M.A. El-Sayed, *Chem. Rev.* 105 (2005) 1025.
2. A.G. Roca, M.P. Morales, K. O’Grady, C.J. Serna, *Nanotechnology* 17 (2006)2783.
3. X. Teng, H. Yang, *Nanotechnology* 16 (2005) S554.
4. X. Cao, L. Gu, *Nanotechnology* 16 (2005)180.

5. S.I. Stoeva, V. Zaikovski, B.L.V. Prasad, P.K. Stoimenov, C.M. Sorenson, K.J. Klabunde, *Langmuir* 21 (2005) 10280.
6. A. Bharde, A. Wani, Y. Shouche, P.A. Joy, B.L.V. Prasad, M. Sastry, *J. Am. Chem. Soc.* 127 (2005) 9326.
7. I. Willner, R. Baron, B. Willner, *Adv. Mater*. 18 (2006) 1109.
8. C. Salzemann, I. Lisiecki, J. Urban, M.P. Pileni, *Langmuir* 20 (2004) 11772.
9. C. Mao, D.J. Solis, B.D. Reiss, S.T. Kottmann, R.Y. Sweeney, A. Hayhurst, G. Georgiou, B. Iverson, A.M. Belcher, *Science* 303 (2004) 213.
10. T.K. Sau, C.J. Murphy, *Langmuir* 20 (2004) 6414.
11. L. Manna, E.C. Scher, A.P. Alivisatos, *J. Am. Chem. Soc*. 122 (2000) 12700.
12. A. Verma, T.C. Goel, R.G. Mendiratta, M.I. Alam, *Mater. Sci. Eng*. B 60 (1999) 156.
13. B. Parvatheeswara Rao, P.S.V. Subba Rao, K.H. Rao, *IEEE Trans. Magn*. 33 (6) (1997) 4454.
14. N. M. Deraz, *J. Anal. Appl. Pyrolysis* 91(2011)48.
15. Q. Liu, J. Sunb, H. Longa, X. Suna, X. Zhonga, Z. Xub, *Mater. Chem. Phys*. 108(2008) 269.
16. O. Carp, L. Patron, A. Reller, *Mater. Chem. Phys*. 101 (2007) 142.
17. W.W.Wang, *Mater. Chem. Phys*. 108 (2008) 227.
18. G. Gnanaprakash, J. Philip, T. Jayakumar, B. Raj, *J. Phys. Chem*. B 111 (2007) 7978.
19. S.H. Xiao,W.F. Jiang, L.Y. Li, X.J. Li, *Mater. Chem. Phys*. 106 (2007) 82.
20. J.M. Hasting, L.M. Corliss, *Phys. Rev*. 102 (1956) 1460.
21. Y.G. Chukalkin, V.R. Shtirts, *Sov. Phys. Solid State* 30 (1988) 1683.
22. W. Schäfer, W. Kockelmann, A. Kirfel, W. Potzel, F.J. Burghart, G.M. Kalvius, A. Martin, W.A. Kaczmarek, S.J. Campbell, *Mater. Sci. Forum* 321–324 (2000) 802.
23. H. F. Yu and K. C. Huang, *J. Magn. Magn. Mater*. 260**(**2003**)** 455.
24. R. D. Purohit, A. K. Tyagi, M. D. Mathews and S. Saha, *J. Nucl. Mater*. 280(2000**)** 51.
25. B.D. Cullity, Elements of X-ray Diffraction, Addison-Wesly Publishing Co. Inc. 1976 (Chapter 14).
26. R. D. Waldron, *Phys. Rev*. 99(1955)1727.
27. N. M. Deraz, *J. Anal. Appl. Pyrolysis* 82(2008)212.
28. Marykutty Thomas, S. K. Ghosh, K. C. George, *Mater. Lett*. 56(2002)386.
29. A. C. F. M. Costa, A. M. D. Leite, H. S. Ferreira, R.H.G.A. Kiminami, S. Cava, L. Gama, *J. Euro. Ceram. Soc*. 28(2008)2033.
30. G. F. Goya, H. R. Richenberg, M. Chen, W.B. Yelon, *J. Appl. Phys*. 87(2000)8005.
31. C. N. Chinnasamy, A. Narayanasamy, N. Ponpandian, K. Chattopadhyay, H. Guerault, J. M. Greneche, *J. Phys. Condens. Matter*. 12(2000)7795.
32. K. Maaz, S. Karim, A. Mumtaz, S.K. Hasanain, J. Liu, J.L. Duan, *J. Magn. Magn. Mater*. 321 (2009) 1838.
33. K. Maaz, A. Mumtaz, S.K. Hasanain, A. Ceylan, *J. Magn. Magn. Mater*. 308 (2007) 289.
34. M.K. Roy, B. Halder, H.C. Verma, *Nanotechnol*. 17 (2006) 232.
35. E. M. Mohammed, K. A. Malini, P. Kurian, M. R. Anantharaman, *Mater. Res. Bull*. 37(2002)753
36. B. D. Cullity, Introduction to Magnetic Materials, Addison-Wesely Publishing Company. Inc, Reading, MA, 1972.
37. S. Chikazumi, Physics of Magnetism, Wiley, New York, 1959.
38. C. Upadhyay, H. C. Verma, V. Sathe, and A. V. Pimpale, *J. Magn. Magn. Mater*. 312(2007)71.